The Astrophysical Journal, 757:41 (11pp), 2012 September 20 doi:10.1088/0004-637X/757/1/41
© 2012. The American Astronomical Society. All rights reserved. Printed in the U.S.A.

ON THE EXCITATION AND FORMATION OF CIRCUMSTELLAR FULLERENES

J. Bernard-Salas[1], J. Cami[2,3], E. Peeters[2,3], A. P. Jones[1], E. R. Micelotta[2], and M. A. T. Groenewegen[4]
[1] Institut d'Astrophysique Spatiale, CNRS/Université Paris-Sud 11, F-91405 Orsay, France; jbernard@ias.u-psud.fr
[2] Department of Physics and Astronomy, The University of Western Ontario, London, ON N6A 3K7, Canada
[3] SETI Institute, 189 Bernardo Avenue, Suite 100, Mountain View, CA 94043, USA
[4] Royal Observatory of Belgium, Ringlaan 3, B-1180 Brussels, Belgium
Received 2012 May 24; accepted 2012 July 23; published 2012 September 4

ABSTRACT

We compare and analyze the *Spitzer* mid-infrared spectrum of three fullerene-rich planetary nebulae in the Milky Way and the Magellanic Clouds: Tc1, SMP SMC 16, and SMP LMC 56. The three planetary nebulae share many spectroscopic similarities. The strongest circumstellar emission bands correspond to the infrared active vibrational modes of the fullerene species C_{60} and little or no emission is present from polycyclic aromatic hydrocarbons. The strengths of the fullerene bands in the three planetary nebulae are very similar, while the ratios of the [Ne III]15.5 μm/[Ne II]12.8 μm fine structure lines, an indicator of the strength of the radiation field, are markedly different. This raises questions about their excitation mechanism and we compare the fullerene emission to fluorescent and thermal models. In addition, the spectra show other interesting and common features, most notably in the 6–9 μm region, where a broad plateau with substructure dominates the emission. These features have previously been associated with mixtures of aromatic/aliphatic hydrocarbon solids. We hypothesize on the origin of this band, which is likely related to the fullerene formation mechanism, and compare it with modeled hydrogenated amorphous carbon that present emission in this region.

Key words: circumstellar matter – infrared: general – ISM: lines and bands – ISM: molecules – planetary nebulae: general – stars: AGB and post-AGB

Online-only material: color figures

1. INTRODUCTION

The C_{60} molecule, buckminsterfullerene, was discovered in laboratory experiments aimed at understanding the formation of long carbon chains in the circumstellar environment of carbon stars and their survival in the interstellar medium (ISM; Kroto et al. 1985). In these experiments, graphite was vaporized in a hydrogen-poor atmosphere using helium as a buffer gas, resulting in clusters of carbonaceous particles of different sizes. Amongst the cluster population, the particles with 60 carbon atoms were the most stable species and the researchers concluded that these species are structured like a truncated icosahedron—often compared to the geometry of a black and white soccer ball. Fullerenes are now known as a class of carbon-based molecules in the shape of a hollow sphere or ellipsoid. Fullerenes can be formed very efficiently in laboratory experiments, converting a few percent of graphite into C_{60} (Krätschmer et al. 1990a, 1990b).

As soon as they were discovered, it was suggested that their extreme stability, in particular against photodissociation, makes fullerenes ideally suited to survive the harsh radiation field in the ISM and thus could be widespread in the galaxy (e.g., Kroto et al. 1985). Once injected into the ISM, they could contribute to interstellar extinction, heating, charge exchange with ions, and providing active surfaces for complex chemical reactions (Kroto & Jura 1992; Foing & Ehrenfreund 1994). They have also been suggested to be responsible for the dust-correlated excess in microwave background radiation observed in some molecular clouds (Watson et al. 2005; Iglesias-Groth 2004, 2006).

Recently, we have detected and identified the vibrational modes of the fullerene species C_{60} and C_{70} in the *Spitzer* Infrared Spectrograph (IRS) spectrum of the young planetary nebula (PN) Tc 1 (Cami et al. 2010, Paper I hereafter). C_{60} has now been detected in many more evolved stars: a handful of PNe in the Milky Way (García-Hernández et al. 2010) and the Magellanic Clouds (García-Hernández et al. 2011a); in the protoplanetary nebula IRAS 01005+7910 (Zhang & Kwok 2011); in the post-AGB stars HD 52961, IRAS 06338+5333 (Gielen et al. 2011), and HR 4049 (Roberts et al. 2012); in the surroundings of a few R Cor Bor stars (Clayton et al. 2011; García-Hernández et al. 2011b); and in the peculiar binary object XX Oph (Evans et al. 2012). These detections suggest that fullerenes are formed by the complex, rich circumstellar chemistry that occurs in the short transition phase from asymptotic giant branch (AGB) star toward PN (Paper I; Zhang & Kwok 2011), or more generally in the circumstellar environments of carbon-rich evolved stars. However, it is not clear how the fullerenes form. Proposed mechanisms include the formation in hydrogen-poor environments, photochemical processing of hydrogenated amorphous carbon (a-C:H or HAC) grains, and high-temperature formation in carbon-rich environments or the formation of fullerenes from the destruction of polycyclic aromatic hydrocarbons (PAHs).

The Infrared (IR) C_{60} bands have also been seen in the interstellar medium and in young stellar objects. Following their earlier suggestions (Sellgren et al. 2007), Sellgren et al. (2010) confirmed the presence of C_{60} in the reflection nebulae NGC 7023 and NGC 2023, and showed that in NGC 7023 the fullerenes emission comes from a different location than that of the PAH bands. Rubin et al. (2011) furthermore report the detection of C_{60} in the Orion nebula, and Roberts et al. (2012) found the C_{60} bands in a few young stellar objects and a Herbig Ae/Be star. These detections show that fullerenes can survive the conditions in the ISM and become incorporated into the regions around young stars and, possibly, planetary systems.

A key question in the studies of fullerenes in astrophysical environments is what drives the excitation of these species. This is fundamentally important, since it determines how the

fullerene bands can be used to probe the physical conditions of the environment in which they reside. While the presence of circumstellar and interstellar fullerenes is now firmly established, many questions about their excitation mechanism remain (see Cami et al. 2011, for a review). Three different mechanisms have been considered. In Paper I, we showed that the relative strength of the C_{60} and C_{70} bands in Tc 1 is consistent with a thermal distribution over the excited states. Such an excitation mechanism could be understood if the fullerenes are not free gas-phase species, but are instead in the solid state or attached to dust grains. Such a solid state origin could also explain the lack of anharmonicities in the band profiles and the apparent lack of ionized fullerenes. Sellgren et al. (2010) and Berné & Tielens (2012) on the other hand assume that the fullerene emission originates from IR fluorescence of isolated free molecules in the gas phase. They compare the band ratios of the 7.0 μm/18.9 μm fullerene bands in their observations to Monte Carlo simulations for stochastic heating and fluorescent cooling, and find agreement for one object but not the other (Sellgren et al. 2010). The third mechanism is based on chemical excitation, and involves H atom recombination in HAC materials (Duley & Williams 2011).

In spite of clear spectral differences resulting from both mechanisms (see Section 4), there is no clear consensus yet on the precise mechanism that operates in the astrophysical environments where fullerenes reside, and observational support for either mechanism can be found. In several cases where the 17.4 and 18.9 μm bands are detected, the 7.0 and 8.5 μm bands are very weak or absent, and this is hard to understand when considering fluorescence. On the other hand, little variation has been reported in the relative band strengths of the 17.4 and 18.9 μm bands, which is hard to understand in the framework of thermal models.

Two contributing factors have hampered progress in determining the excitation mechanism. First, most observations that exhibit the fullerene bands are strongly affected by PAH emission, which makes a good determination of the fullerene band strengths very difficult at best. Second, there is a large scatter in the existing literature about what are the intrinsic band strengths of the fullerene bands. Consequently, the measured observational values could lead to quite different conclusions depending on what intrinsic values are used.

In this paper we analyze and compare the *Spitzer*-IRS spectra of three PNe exhibiting clear and strong emission of circumstellar fullerenes. Two of these PNe, Tc1 and SMP SMC 16, have been published in the literature, while the mid-IR spectrum of the third object, SMP LMC 56, is presented here for the first time. The three PNe are ideally suited to study the excitation mechanism of circumstellar fullerenes: there is no discernible PAH emission present that could have a significant contaminating influence on the fullerene band strengths; the relative strength of the fine-structure lines furthermore indicates that the overall excitation conditions in the three nebulae are different; and we have some additional spatial information for one object (Tc 1). At the same time, the three spectra offer intriguing clues about the formation of circumstellar fullerenes.

This paper is organized as follows. In Section 2, we describe the observations and data reduction steps. Section 3 summarizes what we know about the conditions in the three objects. In Section 4, we investigate the excitation process by comparing the observed fullerene band strengths to thermal and fluorescence models using different literature sources for the intrinsic band strengths. We discuss the formation of fullerenes in Section 5.

2. DATA AND MEASUREMENTS

2.1. Observations

The observations presented here were carried out by the IRS (Houck et al. 2004) on board the *Spitzer Space Telescope* (Werner et al. 2004). The mid-IR spectrum of Tc1 was published by Perea-Calderón et al. (2009) and our group (Paper I) and consists of observations at high resolution covering the 10–36 μm range (using the short-high (SH) and long-high (LH) modules) as well as observations using the short-low (SL) and long-low (LL) modules covering the wavelength range between 5.4 and 36 μm at a variable resolution of 60–120. SMP SMC 16 was part of the sample presented by García-Hernández et al. (2011a) but we have re-extracted its spectrum with our method for consistency. The spectrum of SMP LMC 56 is obtained from the *Spitzer* Archive (AOR key = 22423808, PID = 40159, PI: A.G.G.M. Tielens). Both SMP LMC 56 and SMP SMC 16 were observed at low resolution only using the SL and LL modules.

The data were processed using version S18.7 of the *Spitzer* Science Center's pipeline and, for SMP LMC 56 and SMP SMC16, using the new optimal extraction algorithm in *Smart*[5] (Higdon et al. 2004; Lebouteiller et al. 2010). The extraction procedures for these two objects follow those of our earlier papers (Paper I; Bernard-Salas et al. 2009); we summarize the main steps below.

The data reduction started from the basic calibrated data products, usually referred to as bcd. First, rogue or unstable pixels were removed and replaced using the irsclean tool.[6] Then the different cycles were combined for a given module and order. To remove the background, the nod positions for a given module and order combination where subtracted from each other. There seems to be some extended emission in SMP LMC 56 around 33 μm in the LL1 module, which could affect the [S III] 33.4 μm line. Similarly, this spectrum also shows a slight difference in the absolute flux between nod1 and nod2 in the LL modules ($\sim$12%). None of these affect in any way the conclusions of the paper. The final step is to extract the differenced images. Both objects are a point source for the *Spitzer*-IRS beam and thus we used the optimal extraction algorithm implemented in *Smart*. After optimal extraction, any remaining glitches that may have prevailed from the previous steps were removed manually. Finally, the two nods were combined to increase the signal-to-noise ratio. No scaling was needed between the modules. The resulting spectra are shown in Figure 1.

2.2. The Spectra

To aid further discussions, we provide a brief description here of the different features in the spectra. As can be seen from Figure 1, the spectra of Tc1, SMP LMC 56, and SMP SMC 16 reveal the same overall shape: a strong rising dust continuum on which many emission features are superposed. Some of these are better seen in Figure 2 where we show continuum subtracted, as well as normalized, spectra.

The spectra exhibit many low-excitation fine-structure lines. These show up clearly as narrow lines in the high resolution part of the spectrum of Tc 1 ($\lambda \gtrsim 10\,\mu$m), which makes it straightforward to distinguish them from other spectral features. In the low-resolution observations, the much larger line width

[5] *Smart* can be downloaded from this Web site: http://irsa.ipac.caltech.edu/data/SPITZER/docs/dataanalysistools/contributed/irs/smart/.
[6] This tool is available from the SSC Web site: http://ssc.spitzer.caltech.edu.

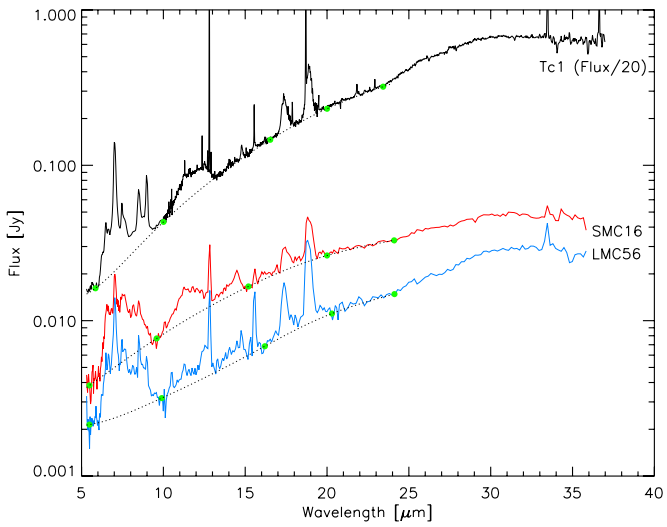

Figure 1. Observed *Spitzer*-IRS spectrum of Tc1 (divided by 20), SMP LMC 56, and SMP SMC 16. The dashed line indicates the adopted dust continuum, and the green dots the anchor points used to define it.

(A color version of this figure is available in the online journal.)

makes it harder to separate the fine-structure lines from other bands. The most prominent lines are [Ar II] (6.99 μm), [Ar III] (8.99 μm), [Ne II] (12.81 μm), [Ne III] (15.55 μm), and [S III] (18.7 μm). A weak [S IV] line at 10.51 μm is present as well. In Tc 1, the [S III] line at 18.7 μm is perched on top of the much broader C_{60} band. In the low-resolution spectra of SMP LMC 56 and SMP SMC 16, the presence of the [S III] can be inferred from band asymmetries (see the Appendix). We note that the 34.8 μm line of [S III] in SMP LMC 56 is contaminated by the extended emission mentioned in Section 2.1, and we cannot determine how much of it originates from the actual source.

These spectra furthermore clearly show fullerene emission bands, and it is remarkable how similar the relative strengths of the fullerene bands are in these three PNe (Figure 2, top). There is little to no contamination by PAH features, and thus these three objects represent some of the clearest detections of fullerenes. Most notable are the strong and broad C_{60} bands at 7.0, 8.5, 17.4, and 18.9 μm. Tc1 furthermore also exhibits weaker features at 12.7, 14.8, 15.6, and 21.8 μm that are attributed to C_{70} (Paper I); C_{70} also contributes ($\sim$10% of the total power) to the 17.4 and 18.9 μm bands. These features could be present in the spectrum of SMP LMC 56, but seem absent in SMP SMC 16.

Individually, the spectra show little evidence for the presence of PAHs, which are typically seen in carbon-rich PNe. However, the three spectra do show a weak bump at 11.3 μm; emission at these wavelengths is generally attributed to PAHs. SMP LMC 56 also shows a feature near 12.7 μm where another PAH band is commonly seen; however, in our case, this feature may be due to C_{70}. Other PAH bands are not easily identified. Notably absent is the usually strong 7.7 μm PAH band. There is a very weak bump near 6.2 μm in Tc1 and SMP LMC 56, which is not clear or present in SMP SMC 16 while any possible 8.6 μm PAH emission will be blended with the C_{60} feature.

Very striking in the spectra of all three PNe are the broad emission plateaus between 6 and 9 μm and between 10 and 13 μm. Similar plateaus in these spectral regions have been attributed to modes of alkane and alkene groups on the periphery of polycyclic aromatic systems in proto-PNe by Kwok et al. (2001). The 6–9 μm plateau is seen in very few other PNe and could thus well be related to the fullerene formation process. In fact, García-Hernández et al. (2010) hypothesize that these

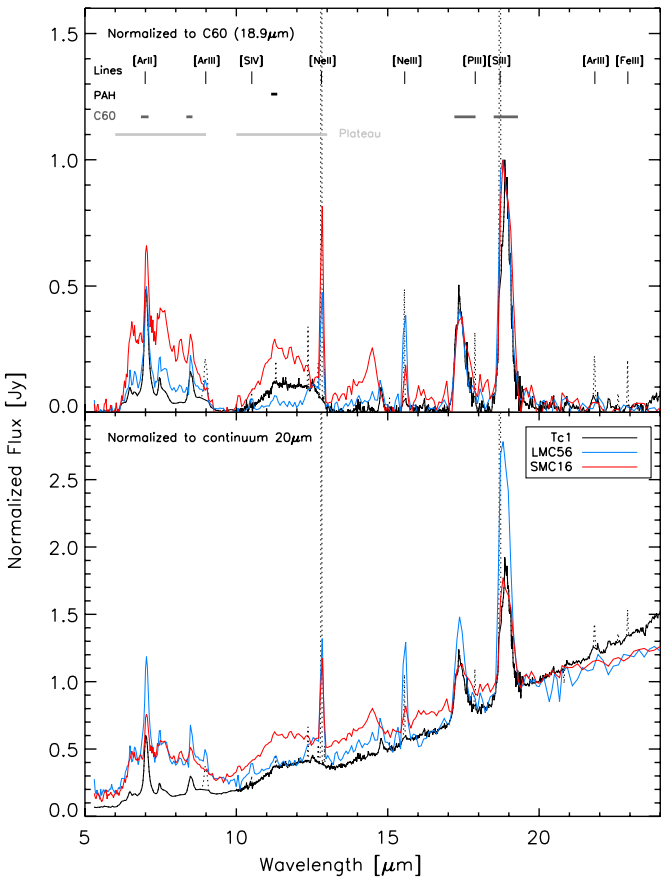

Figure 2. Top panel: continuum-subtracted spectra of the 5–24 μm region normalized to the peak of the 18.9 μm feature. Atomic fine-structure lines in Tc 1 are shown as dotted lines. Bottom panel: spectra normalized to the 20 μm continuum flux. As can be seen, the three PNe have very similar continuum emission.

(A color version of this figure is available in the online journal.)

features are due to HACs, and that fullerenes are formed from the decomposition of these HAC grains. We discuss this further in Section 5. In this paper we use the term HAC in its broader sense to include the whole family of these materials (e.g., petroleum, coals, quenched carbonaceous composite a-C:H, a-C, etc.).

The 6–9 μm plateau reveals some substructure as well. This substructure is present in both nod positions, and in each of the three objects confirming that these are real spectral features. Tc 1 and SMP LMC 56 have features at 6.49 and 6.65 μm. These are also observed in a few post-AGB stars (Gielen et al. 2011). In addition, there is a fairly broad feature between roughly 7.35 and 7.85 μm best seen in SMP SMC 16 and SMP LMC 56. The width of the feature is about the same as that of the C_{60} bands. It is interesting to note that 7.5 μm is about the wavelength where a C_{60}^{+} band is expected (Fulara et al. 1993). Tc1 and SMP LMC 56 also show a small peak at about 7.48 μm, most likely due to the H I recombination line. Finally, SMP LMC 56 and SMP SMC 16 show a feature at 8.15 μm that is not present in Tc1.

The plateau emission in the 10–13 μm region is quite strong in Tc 1 and SMP SMC 16, and weaker in SMP LMC 56. A 10–13 μm emission plateau is also observed toward other PNe (Bernard-Salas et al. 2009) and is generally attributed to SiC (Speck et al. 2005, 2009). However, the profile of the plateau in our three PNe is quite different from those PNe, and suggests that here, a different carrier might be responsible.

In all three sources, we also detect the so-called 30 μm feature that is commonly seen in carbon-rich PNe. This feature is often

Table 1
Flux Measurements (All Values in W m^{-2})

	Tc 1	SMC 16	LMC 56
$F_{\rm dust}$	6.0×10^{-13}	4.5×10^{-15}	1.9×10^{-15}
[Ne II] (12.8 μm)	2.3×10^{-14}	3.5×10^{-17}	2.1×10^{-17}
[Ne III] (15.5 μm)	8.9×10^{-16}	7.7×10^{-18}	1.8×10^{-17}
18.9 μm band			
Total[a]	2.4×10^{-14}	9.5×10^{-17}	9.3×10^{-17}
[S III][b]	8.7×10^{-15}	3.4×10^{-17}	3.4×10^{-17}
Fullerenes[b]	1.4×10^{-14}	4.1×10^{-17}	4.4×10^{-17}
Baseline[b]	2.0×10^{-15}	2.0×10^{-17}	1.5×10^{-17}
C_{70}[c]	$\sim 1.4 \times 10^{-15}$		
C_{60}	1.3×10^{-14}	5.1×10^{-17}	5.2×10^{-17}
Uncertainty[d]	1×10^{-15}	1×10^{-17}	8×10^{-18}
17.4 μm band			
Total[a]	9.2×10^{-15}	4.3×10^{-17}	4.3×10^{-17}
Contaminants[e]	6.1×10^{-16}		
Baseline	1.2×10^{-15}	1.3×10^{-17}	1.6×10^{-17}
C_{70}[c]	$\sim 1.8 \times 10^{-15}$		
C_{60}	6.2×10^{-15}	3.7×10^{-17}	3.5×10^{-17}
Uncertainty[d]	6×10^{-16}	7×10^{-18}	8×10^{-18}
8.5 μm band			
C_{60}	3.9×10^{-15}	1.8×10^{-17}	1.3×10^{-17}
Uncertainty[d]	2×10^{-16}	3×10^{-18}	3×10^{-18}
7.0 μm band			
Total[a]	2.1×10^{-14}	6.8×10^{-17}	9.0×10^{-17}
[Ar II][b]	3.4×10^{-15}	2.5×10^{-17}	...
C_{60}	1.7×10^{-14}	4.1×10^{-17}	9.0×10^{-17}
Uncertainty	3×10^{-15}	1×10^{-17}	1×10^{-17}
$F(17.4\,\mu m)/F(18.9\,\mu m)$	0.47 ± 0.06	0.72 ± 0.29	0.68 ± 0.18
$F(8.5\,\mu m)/F(18.9\,\mu m)$	0.29 ± 0.02	0.36 ± 0.09	0.26 ± 0.05
$F(7.0\,\mu m)/F(18.9\,\mu m)$	1.31 ± 0.28	0.80 ± 0.42	1.74 ± 0.63

Notes.
[a] From integrating over the entire band.
[b] From fitting the observations with two Gaussian profiles and a linear baseline.
[c] Estimate from Paper I.
[d] Mainly due to mispositioning continuum.
[e] For Tc 1: the [P III] line and a weaker line at 17.6 μm.

attributed to MgS (Hony et al. 2002; Bernard-Salas et al. 2009), but could also have a carbonaceous origin (e.g., Volk et al. 2011). Finally, SMP SMC 16 shows an asymmetric feature that peaks at 14.5 μm; it is not clear what the origin is of this feature.

2.3. Flux Measurements

Detail information on how the different features (continuum, atomic lines, fullerene bands) were measured is given in the Appendix, and these values are listed in Table 1.

For what follows, the most important quantities are the flux ratios of the different C_{60} bands. We have included in Table 1 the band ratios normalized to the 18.9 μm band. It is immediately clear that the derived $F(8.5\,\mu m)/F(18.9\,\mu m)$ ratios are very similar, and are in fact compatible with a constant ratio equal to the weighted mean value of 0.29 ± 0.02. The $F(17.4\,\mu m)/F(18.9\,\mu m)$ ratio shows a somewhat larger spread but also larger uncertainties. The weighted mean value is 0.50 ± 0.06, and all measurements are thus consistent with a constant value. For the ratios involving the 7 μm band, there is a much larger spread in the resulting band ratios, which stems to a large degree from the difficulties in determining the contribution of the [Ar II] line to the 7 μm emission. The weighted mean ratio is 1.22 ± 0.22, and given the uncertainties, it is not clear whether any real variations are present.

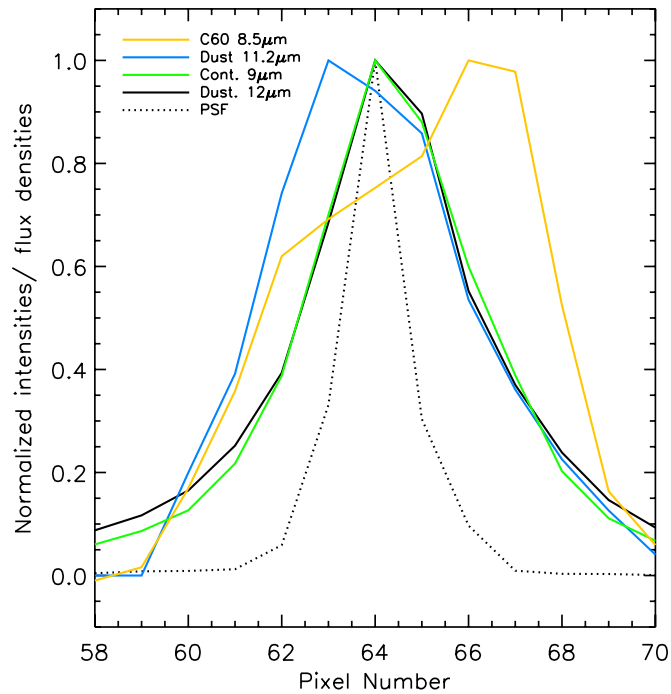

Figure 3. Spatial distribution of different dust components in Tc1 along the SL slit. The point-spread function (PSF) is shown for reference. The central star is located at pixel 64. All components are extended; but whereas the dust continuum emission is roughly centered on the star, the fullerene emission peaks 2–3 pixels away (to the right in this figure) from the central star. The 11.2 μm feature peaks about a pixel away from the central star on the other side of the fullerene emission.

(A color version of this figure is available in the online journal.)

In Table 1 we furthermore list the fluxes of the [Ne II] (12.8 μm) and [Ne III] (15.5 μm), fine-structure lines that will be of importance later on.

2.4. Spatial Distribution

Because of its proximity and size ($\sim 9''$), we can study the spatial distribution of several emission components in Tc 1 relative to the position of the central star in the SL slit ($1\farcs8$ per pixel in the spatial direction; Figure 3); unfortunately, this is not possible for the high-resolution observations nor for the much more distant SMP SMC 16 and SMP LMC 56. We mapped the distribution of the thermally emitting dust by using the flux at 9.46 μm. From Figure 3, it is clear that the dust emission is extended and centered on the central star. The same holds true for the flux at 12 μm, which traces the dust continuum in addition to the broad 10–13 μm plateau (see Figure 2). The emission in the 8.5 μm fullerene band and in the weak 11.2 μm feature is even more extended. However, in both cases, the emission is displaced from the central star and the two different components peak at opposite direction from the central star. This is reminiscent of the reflection nebulae NGC 7023 and NGC 2023 where Sellgren et al. (2010) and Peeters et al. (2012) reported a similar spatial separation in the distribution of fullerene and PAH emission. The 2–3 pixel displacement of the fullerene emission corresponds to 6400–9700 AU at the distance of Tc 1 (1.8 kpc; Pottasch et al. 2011).

3. NEBULAR CONDITIONS

As hinted at by their spectroscopic resemblance, Tc1, SMP LMC 56, and SMP SMC 16 share some physical properties. The

observed line emission is dominated by low-excitation lines, typical of low-excitation PNe. The dust emissions starts to rise at <5 μm, indicating the presence of a hot dust component. This continuum emission is typical and similar to other young PNe like NGC 7027 and BD+30 3639 (Bernard-Salas et al. 2003; Bernard-Salas & Tielens 2005). Further evidence for a young age is the fact that Tc1 and SMP SMC 16 are relatively compact objects. Furthermore, the effective temperatures ($T_{\rm eff}$) of the central stars are low. Tc1 has a $T_{\rm eff}$ of 34,700 K and SMP SMC 16 of 37,000 K (Dopita & Meatheringham 1991; Pottasch et al. 2011). Villaver et al. (2003) note that the Zanstra temperature in SMP LMC 56 is low (45,900 and 29,000 K for He II and H I, respectively), and places the object in the early stages of the Helium burning tracks of Vassiliadis & Wood (1994), again indicating that it is young. The electron temperatures are: 9000 K for Tc1 (Pottasch et al. 2011), ~13,100 and 11,800 K for SMP LMC 56 and SMP SMC 16, respectively (Leisy & Dennefeld 2006). These are not very high when compared to other PNe in their host galaxies (see, e.g., samples by Stanghellini et al. 2007; Bernard-Salas et al. 2009).

Tc1 and SMP SMC 16 are carbon-rich, with high C/O ratios of 1.4 and 2.1, respectively (from abundances by Pottasch et al. 2011; Stanghellini et al. 2009; Leisy & Dennefeld 2006). There are no carbon abundances available in the literature for SMP LMC 56 but its mid-IR spectral characteristics are clearly that of a carbon-rich environment (e.g., presence of fullerenes, 30 μm feature). As it has been suggested before, these conditions (young, carbon-rich, low excitation) appears to favor the formation of fullerenes.

Although the conditions in the three PNe are quite similar, they are not the same. In particular, the observed line emission suggests that the overall excitation conditions are somewhat different. This follows from the [Ne III]/[Ne II] ratio, which is an indicator for the strength of the radiation field and which changes significantly—from about 0.04 in Tc 1 to 0.22 in SMP SMC 16 and to 0.86 in SMP LMC 56.

4. THE EXCITATION OF CIRCUMSTELLAR FULLERENES

4.1. Thermal and Fluorescence Models

We start our analysis from the *intrinsic* relative strengths for the C_{60} bands. The literature offers quite a few sources where band strengths have been obtained theoretically or experimentally, and there is a fair amount of disagreement in the relative strengths of the C_{60} bands. Here, we have chosen four different literature sources (Chase et al. 1992; Fabian 1996; Choi et al. 2000; Iglesias-Groth et al. 2011) from both theoretical and experimental results, which together are fairly representative of the band strength differences found in the literature. The band strengths (relative to 18.9 μm band) are listed in Table 2. All sources agree that the 18.9 μm band is the strongest, and that the 8.5 μm band is the weakest, but there is disagreement about the rest, with differences in the actual listed values of up to a factor 2.5 (for the 17.4 μm band).

In the thermal models considered so far, the emitted power in each of the C_{60} bands is proportional to the population in the corresponding excited vibrational state, and this in turn is set by the temperature through the Boltzmann equation. These models thus assume that the emission is optically thin, and that emission from hot bands can be neglected. Certainly for high temperatures, this latter approximation is questionable. Thermal models show that the strength of the 17.4 μm band (relative to the 18.9 μm band) changes significantly as a function of temperature for $T \lesssim 500$ K, and furthermore that the 7.0 and 8.4 μm bands are weak or absent for $T \lesssim 300$ K (see Figure 4).

Table 2
Intrinsic and Observational Values for the Band Strengths Relative to the $T_{1u}(1)$ Band at 18.9 μm; Derived Temperature Ranges and Ranges in Photon Energies

	$T_{1u}(2)$ (17.4 μm)	$T_{1u}(3)$ (8.5 μm)	$T_{1u}(4)$ (7.0 μm)
	Relative Band Strength		
Intrinsic (literature)			
Choi	0.26	0.31	0.46
Chase	0.34	0.28	0.34
Fabian	0.48	0.45	0.38
Iglesias-Groth	0.66	0.30	0.50
Observational (mean)	0.50	0.29	1.22
	±0.06	±0.02	±0.22
	Derived Parameters		
Thermal models: 1σ temperature ranges (K)			
Choi	···	370–390	585–700
Chase	···	385–405	680–840
Fabian	200–630	320–340	645–785
Iglesias-Groth	105–165	375–395	565–670
Fluorescence models: 1σ photon energies (eV)			
Choi	···	2.7–3.3	11.7–22.8
Chase	···	3.0–3.7	19.0–44.9
Fabian	0.1–50	1.6–2.0	15.9–34.6
Iglesias-Groth	···	2.8–3.4	9.9–18.5

The starting point for IR fluorescence models on the other hand is the absorption of a single UV photon of energy φ that results in an electronic transition. On ultra-short timescales, the absorbed energy is redistributed over the vibrational modes, which causes the molecule to relax back into the electronic ground state, but leaves it in highly excited vibrational states. The molecule then cools by emitting IR photons as it cascades down the energy ladder. The resulting IR spectrum can be calculated in different ways; we follow the approach that is used for calculating the IR fluorescence of PAHs (see, e.g., Allamandola et al. 1989; d'Hendecourt et al. 1989; Bakes et al. 2001; Bauschlicher et al. 2010). The resulting model spectra are equivalent to those obtained, e.g., by a Monte Carlo method (Joblin et al. 2002; Sellgren et al. 2010). Fluorescence models result in a nearly constant $F(17.4\,\mu\text{m})/F(18.9\,\mu\text{m})$ band strength ratio, even for photon energies as low as 1 eV; for realistic values of φ (5–10 eV), the 7.0 and 8.5 μm bands are furthermore fairly strong compared with 18.9 μm band (see Figure 4).

Duley & Williams (2011) proposed that HAC particles can be heated by the recombination of trapped (physisorbed) H atoms with dangling bonds in the HAC structure. The release of chemical energy upon bond formation heats the dust and provides an additional means of exciting the *UIR* bands. Given that the HAC/a-C:H dust in these regions is rather warm (100–150 K), any interstitial H atoms may not be retained within the material. In the following section, we consider the thermal and fluorescence mechanisms.

4.2. Models versus Observations

For each set of intrinsic band strengths listed in Table 2, we have calculated thermal models (for temperatures between 50 K and 1000 K) and fluorescence models (for photon energies between 1 and 15 eV) and calculated the band strength ratios

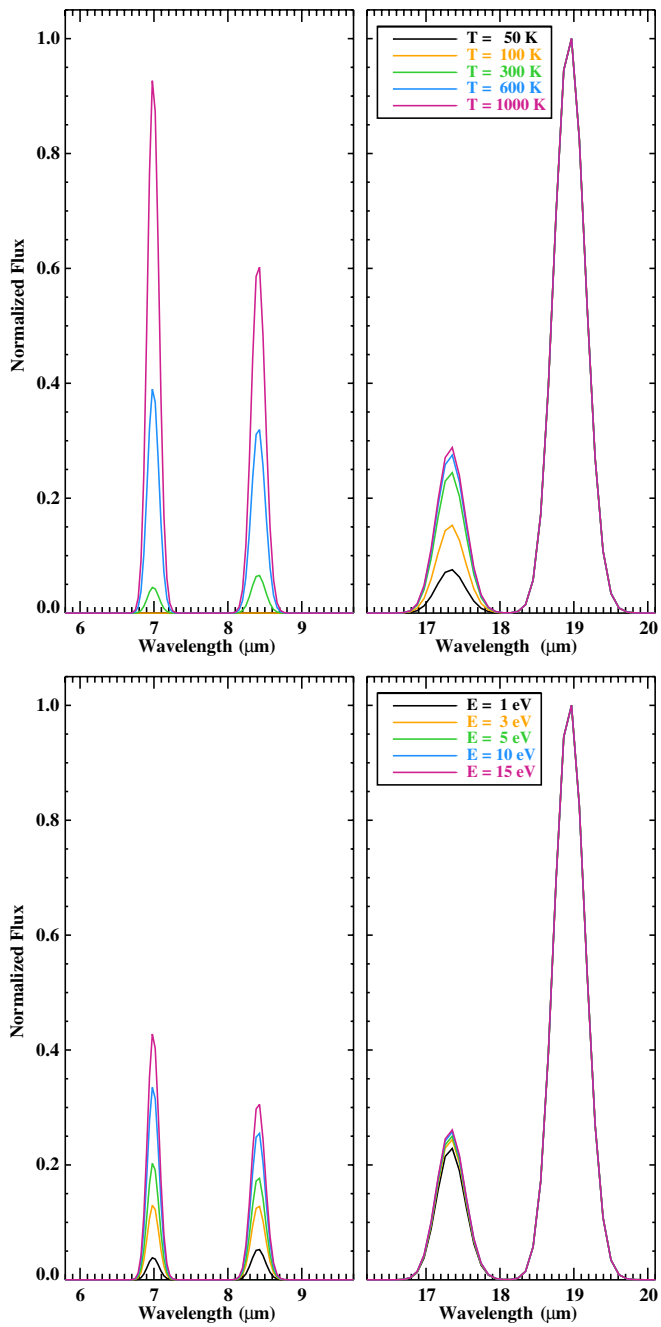

Figure 4. Illustration shows how the relative strengths of the C_{60} bands change as a function of temperature for thermal models (top) and as a function of the average absorbed photon energy for IR fluorescence models (bottom). In all cases, we used the intrinsic band strengths from Choi et al. (2000), and distributed the total power over Gaussian profiles whose width is set by the resolution (taken to be $R = 90$). All figures are normalized to the peak emission in the 18.9 μm band. Note that in the observations presented here, the bands at 17.4 and 18.9 μm are much broader than the instrumental resolution and thus these figures cannot be directly compared to the observations. We did not include temperature-dependent broadening or shifting of the bands.

(A color version of this figure is available in the online journal.)

for each of those models. Figure 5 shows the locus of expected strengths of the 8.5 μm and 17.4 μm bands (normalized to the 18.9 μm band) for all models, and compares these to the observed values for all three PNe (and their weighted mean). Since the lowest point on the thermal model curves in the diagram corresponds to 300 K, there is little variation left in the 17.4 μm band strength for higher temperatures, and the thermal and fluorescence models almost overlap. Based on the strength of the 17.4 μm band, it would thus be impossible to differentiate between thermal and fluorescence models for this range of parameters. Note also how far apart the four different sets of models are, resulting from the very different intrinsic strengths of the 17.4 μm band in the four sets.

The 8.5 μm band has more diagnostic power. From Figure 5 it is clear that already at unrealistically low photon energies of 1 eV (the lowest point on the curves), the fluorescence models predict a band at 8.5 μm that is about 10%–20% of the 18.9 μm band. For more reasonable values of the absorbed energy (5–10 eV), the 8.5 μm band should be about 40%–60% of the 18.9 μm flux. However, the measured ratio is 0.29 ± 0.02, which then implies a low photon energy ($\varphi \approx 3$ eV). In fact, for Tc 1 (and the weighted mean value), we can exclude excitation by 5 eV photons at the 5σ (or better) confidence level, independently of the chosen source of intrinsic band strengths. Such low photon energies would be very hard to understand since it would imply that the fullerenes do not get excited through their strong electronic transitions at UV wavelengths in spite of a strong radiation field. Since this result holds for all sources of intrinsic strength, and the 8.5 μm band strength is well determined (i.e., it is not possible that we miss a large fraction of the flux in this band), the 8.5 μm band strength thus excludes quite strongly the possibility that the observed fullerene emission is due to fluorescence by isolated molecules in the gas phase. Note that for the 7.0 μm band (Figure 6), the same conclusion holds, but then for opposite reasons: Explaining the observed 7.0 μm band strength requires unreasonably high energies for the exciting photons.

Thermal models on the other hand require a temperature in the range 300–400 K to explain the 8.5 μm band strength, which at first sounds reasonable. However, since the relative strength of the 8.5 μm band is nearly the same in all three objects, this implies that also the fullerene temperatures are nearly exactly the same in all three sources; this would be either very coincidental, or an important factor in explaining the presence of fullerenes. Furthermore, the observed 7.0 μm flux is much higher than would be expected for thermal excitation, and this holds for all sources of band strength. Thus, the observations are only consistent with thermal models if the 7.0 μm band would be primarily due to [Ar II] and only a small fraction of the 7.0 μm flux could be attributed to C_{60}. In such a case, the intrinsic strengths listed by Fabian (1996) are fully consistent with the observations (which were the values we used in Paper I). However, we do not believe this to be the case (see the Appendix)—most of the 7.0 μm seems to be originating from C_{60}. Thus, we have to conclude that neither thermal nor fluorescence models can explain the observations completely.

4.3. Discussion

In spite of the difficulties in reconciling the observations with models, the three spectra presented here offer important clues to the excitation mechanism. An important ingredient in understanding the excitation of fullerenes in our sources is the spatial distribution of some of the spectral components in Tc 1 (Section 2.4 and Figure 3). As we discussed, the C_{60} emission peaks at a distance of about 8000 AU from the central star. Given the central star's effective temperature of $T_{\rm eff} \approx 30{,}000$ K, classical "graphitic" dust in equilibrium with the radiation field would be very cold, with temperatures of only 20–25 K. However, we find that hydrogen-rich HAC nanoparticles can

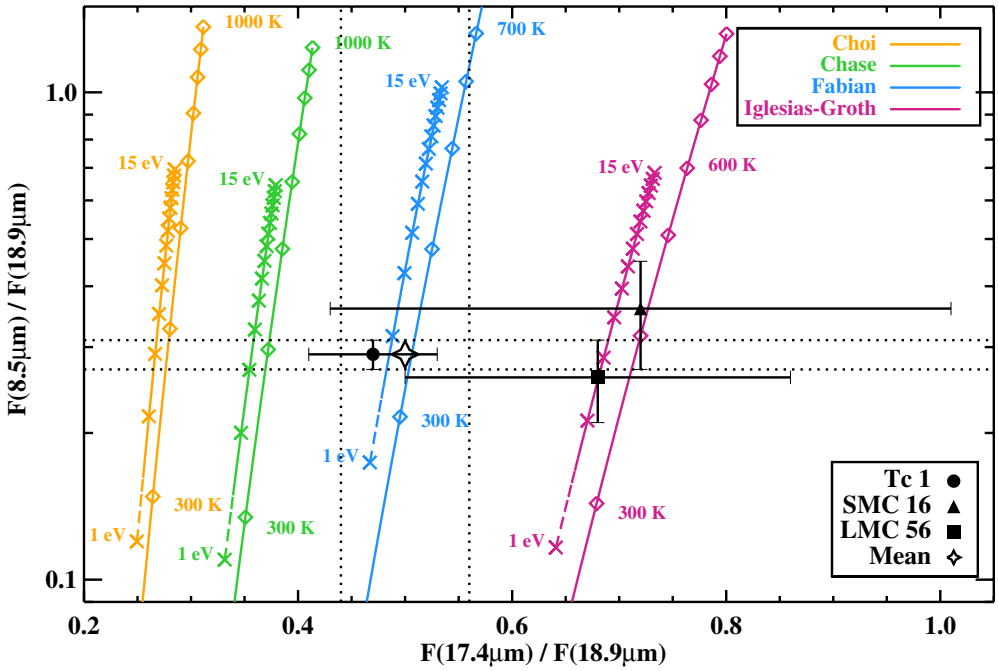

Figure 5. Diagnostic plot showing measurements and different model values for the total flux in the 8.5 μm band and the flux in the 17.4 μm band (both normalized to the 18.9 μm band). Each pair of curves corresponds to a different source of C_{60} band strengths. The right-hand curve for each pair corresponds to the band ratios for thermal models. The diamond plot symbols correspond to temperature increments of 100 K, and a low and a high temperature value is indicated on each curve. The left-hand curves are model values for IR fluorescence. The crosses correspond to increments in the average absorbed photon energy of 1 eV. For each curve, the 1 eV and 15 eV models are indicated. We also show the measured band ratios for each of our three PNe, and the weighted mean value of the band ratios. The dotted lines indicate the 1σ confidence intervals for the mean values.

(A color version of this figure is available in the online journal.)

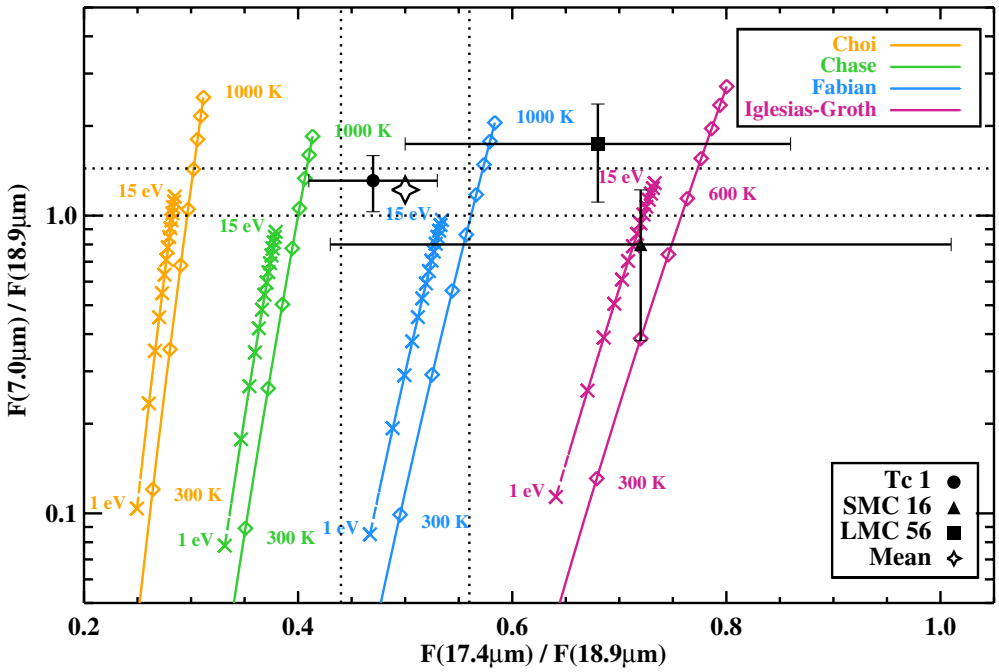

Figure 6. Same as Figure 5, but for the 7.0 μm band instead of the 8.5 μm band.

(A color version of this figure is available in the online journal.)

be maintained at temperatures of 100–150 K at distances of 3000 to 10,000 AU because of their low emissivities at far-infrared wavelengths. This is still not sufficient to heat the fullerenes to the required thermal temperatures of ∼300 K. The spatial information thus rules out thermal emission, and favors fluorescence. For fluorescence, the average photon energy φ absorbed by the molecules is a function of the local radiation field and the absorption cross section of the molecule; this then quite naturally explains why the fullerene band strengths are so similar in the three objects since their central stars have comparable effective temperatures and thus the average absorbed photon energy is very similar as well; for thermal

models such a coincidence would required fine-tuned conditions in all three PNe.

However, as we discussed above, the observations are not consistent with models for fluorescent IR emission either: for realistic energies, all models for fluorescence predict a much stronger 8.5 μm band and a much weaker 7.0 μm band (all relative to the 18.9 μm band) than is observed, and this is the case for all sources of intrinsic band strength. Note that the normalization to the 18.9 μm band in itself is not the issue either—if the 18.9 μm band would be weaker than we measure, this could conceivably bring the 8.5 μm band flux in agreement with models, but then the problem with the 7.0 μm band would even be worse.

Since it is clear that we are not seeing emission from isolated, free C_{60} molecules, an obvious first question is whether we're maybe seeing emission from fullerene clusters or nanocrystals. Such entities that are larger than single molecules could still undergo single-photon heating and IR fluorescence through the same vibrational modes, but their larger heat capacity would result in different band ratios—with lower fluxes at shorter wavelengths. This could possibly explain the discrepancy for the 8.5 μm band, but not for the 7.0 μm band, where the problem would be even bigger.

It is instructive to look at the issue starting from the 8.5 μm band, since this band does not seem contaminated by other emission components. The problem is then that both the observed 18.9 μm and the 7.0 μm bands are too strong to be explained by fluorescence of free isolated C_{60} molecules. This then indicates that other materials are contributing to the 7.0 and 18.9 μm band. For the 18.9 μm band we have already identified one contributor: C_{70}. Given the strength of the other C_{70} bands in the same wavelength range (for Tc 1), it seems unlikely though that we severely underestimate its contribution to the 18.9 μm band; to explain the discrepancies, we would require roughly four times more C_{70} than we have currently estimated. For the 7.0 μm band on the other hand, we have not considered a possible contribution of C_{70} yet. The intrinsically strongest C_{70} band occurs indeed near 7.0 μm. When using thermal models at the fairly low temperatures we derived in Paper I, the transitions at the shorter wavelengths are suppressed significantly, to the point where this band becomes unmeasurably weak. When using fluorescence models however, this is not the case, and based on the intrinsic strength of the band, it could well be responsible for a large fraction of the observed discrepancy. Note that C_{70} still has other features at wavelengths between 5 and 10 μm that should then be reconsidered in the framework of fluorescence, and it is not clear whether attributing the 7.0 μm flux to C_{70} is consistent with the expected strengths of these features.

5. HACs AND THE FORMATION OF FULLERENES

The three spectra we present here also offer intriguing clues to the formation of circumstellar fullerenes. Indeed, as we discussed in Section 2, the three PNe share other notable spectral features in addition to the fullerene bands. Of particular importance for the discussion on fullerene formation mechanisms are the plateaus. Several formation routes are possible in the laboratory or have been proposed, including: (1) low-temperature formation in the absence of hydrogen (Kroto et al. 1985); (2) high-temperature ($T \gtrsim 3000$ K) formation in which case hydrogen may be present (Jäger et al. 2009); (3) photochemical processing of HAC (Scott et al. 1997); and (4) destruction of PAHs (Cami et al. 2011; Berné & Tielens 2012). The plateaus are particularly interesting in this context since Stanghellini et al. (2007) attribute the 6–9 μm and 10–13 μm broad features in their sample of PNe to unprocessed clusters of small carbonaceous grains and/or large PAH clusters. García-Hernández et al. (2010) on the other hand propose that these are due to HACs, which they then suggest become photochemically processed to produce the fullerenes.

In Figure 7 we show the 6–14 μm IR spectra of Tc1, SMP LMC 56, and SMP SMC 16 compared to the IR spectra of HAC/a-C:H particles with a radius of 3 nm at a temperature of 200 K and with varying atom hydrogen fractions of 0.23, 0.29, and 0.35; this is equivalent to band gaps of 1.0, 1.25, and 1.5 eV, respectively (Jones 2012c). The spectra of these particles are dominated by aliphatic and aromatic CC and CH bands (Kwok et al. 2001; Buss et al. 1990). As shown by Jones (2012b, 2012c) these materials appear to also contain few olefinic bands. The overlapping of the aliphatic, aromatic, and olefinic bands results in a plateau-like region underlying the C_{60} 7.0 and 8.5 μm bands and also in bands in the 11–13 μm plateau region.[7] We note that the shape of the continuum matches the observed 6–9 μm plateau emission under the fullerene bands and the atomic lines rather well in these continuum-subtracted spectra. These spectral bands, underlying the fullerene bands, appear to be rather invariant from source to source, suggesting that the particles responsible for these plateaus are therefore small enough to be stochastically heated. However, there is a band at 6.5 μm in the observed spectra that we are unable to identify.

The spectra of Tc1, LMC56, and SMC16 appear to be consistent with these H-rich carbonaceous materials (H atomic fraction 0.35–0.47). Since exposure to UV radiation tends to reduce the hydrogen content of these HAC/a-C:H particles and aromatize the carbonaceous content, this indicates that the particles have not been long-exposed to a strong radiation field. In the diffuse ISM, where the dust is exposed to UV irradiation for millions of years, the small HAC/a-C:H particles are expected to be H-poor, with an H atom fraction of the order of only 0.05 (e.g., Jones 2012a, 2012b). Typical PAHs (i.e., meaning strictly pure aromatics) can be ruled out based on the presence of aliphatic bands in the 6–9 μm spectral region and the shape of the 11–13 μm plateau.

One possible scenario that could therefore explain the particularity of the fullerene sources is that small carbonaceous HAC/a-C:H particles have recently emerged, either by being released from larger (coagulated/accreted) particles or by the ablation of matter from a denser medium, where the a-C:H materials were H-rich. Thus, the carbonaceous dust in these sources would appear to be rather young, in that it has not yet been exposed to stellar radiation for long enough for it to be significantly dehydrogenated and aromatized. This could be understood in the context of optically thick dust not allowing the UV radiation to penetrate until very recently, on its way to becoming optically thin. It is perhaps these conditions that are conducive to fullerene molecule formation by a top-down formation from much larger, three-dimensional carbonaceous particles (e.g., Micelotta et al. 2012) rather than via the PAH-warping mechanism proposed by Berné & Tielens (2012).

As we saw in Section 3 the central stars of the three PNe have similar (low) effective temperatures (~30,000–45,000 K). So far, fullerenes have been detected in low-excitation environments (e.g., proto-PNe, reflection nebulae, YSOs). The link

[7] Longward of 10 μm the strength of the bands is not well characterized. The comparison of the observations and models in this region remains qualitative, particularly in terms of the band strengths.

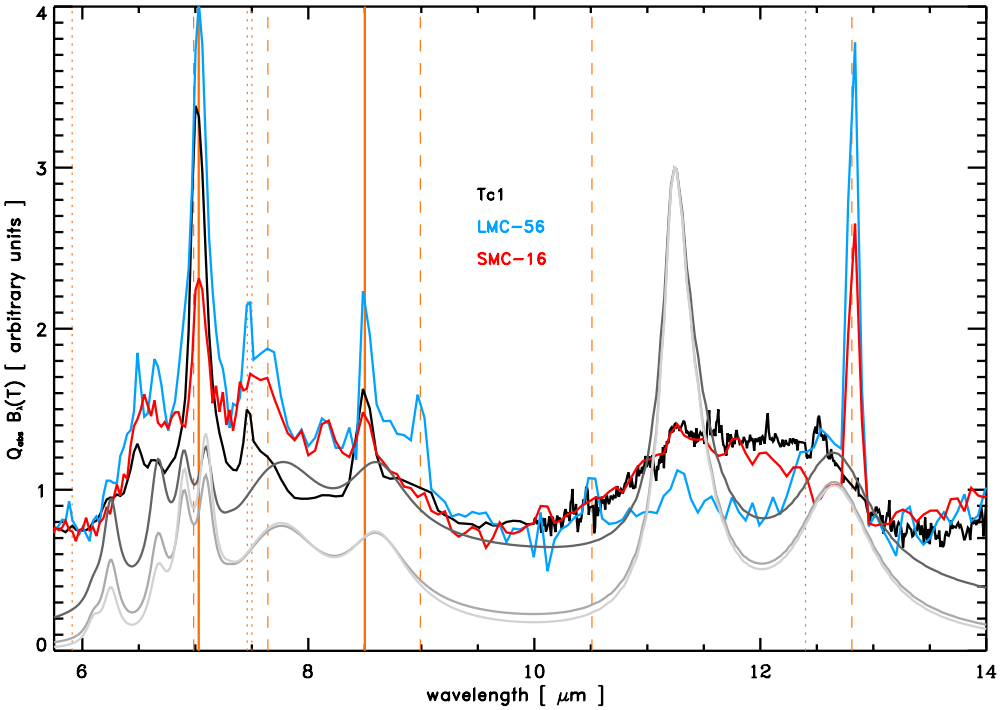

Figure 7. Continuum-subtracted spectra of the fullerene sources (Tc1, LMC 56, and SMC 16 as black, blue, and red lines, respectively) compared to the absorption coefficient, $Q_{\rm abs}$, multiplied by a blackbody, $B_\lambda(T)$, at $T = 200$ K, for 3 nm a-C:H particles with atom hydrogen fractions of 0.23 (dark-gray), 0.29 (mid-gray), and 0.35 (light-gray; Jones 2012c). The vertical orange lines indicate the central positions of the fullerene bands (solid), gas phase ionic (dashed), and hydrogen lines (dotted).

(A color version of this figure is available in the online journal.)

with low-excitation environments has been noted by Evans et al. (2012) in their study of R Coronae Borealis stars. As discussed in Micelotta et al. (2012), fullerene formation is not favored in very low $T_{\rm eff}$ sources because of the lack of sufficient UV photons to dehydrogenate and heat the dust. If it is too high however, fullerenes may not be formed because H-rich carbonaceous particles are destroyed before they can form fullerenes. Conversely, the fullerenes would be ionized, in which case they have many more bands and their emission will be diluted making them much more difficult to detect. It is important to note that not all low-excitation PNe show fullerene emission and so other factors may play a role in the formation/destruction of fullerenes.

6. SUMMARY

We have analyzed and compared the mid-IR spectrum of the three fullerene-rich PNe (Tc1, SMP SMC 16, and SMP LMC 56) to study the fullerene excitation conditions and formation mechanisms. The PNe are low-excitation and carbon-rich nebulae with low electron temperature and thus are presumably young. While other factors may be involved, these conditions seem to favor fullerene formation.

Spectroscopically, these unique PNe share many properties: They show the strongest and clearest circumstellar fullerene bands (C_{60}) detected so far while showing little to no evidence for PAH emission. In addition, they all have strong broad bands in the 6–9 μm and 10–13 μm range, a similar shape of the dust continuum emission, and emission of the so called 30 μm emission feature. The observed fullerene band strengths in the three sources are fairly similar (within uncertainties) as well. However, the intensity of the radiation field in these objects (as inferred by the fine-structure line ratio [Ne III]15.5 μm/[Ne II]12.8 μm) varies by more than a factor 10. Furthermore, the spatial profile of different dust components in Tc 1 indicates that the fullerene emission (C_{60}) peaks far away (6300–9700 AU) from the central source. All this is hard to reconcile with a thermal origin for the fullerene excitation, and thus favors fluorescence as the excitation mechanism. Fluorescence of free, isolated C_{60} molecules would be consistent with the observed band ratios if fluorescent emission from C_{70} contributes significantly to the 7.0 μm band. Additional emitting materials could also be present and this needs to be further investigated.

It is likely that the observed broad bands at 6–9 and 10–13 μm are related to the fullerene formation process. We present model spectra of HAC particles of 3 nm and show that these can reproduce the 6–9 μm band with some degree of success, which may imply that fullerenes are formed by photochemical processing of HAC.

The detection of C_{60} and other unidentified features in these nebulae is very intriguing. Additional information and a larger sample are required to discern the mechanisms that trigger fullerene formation, and set their importance and role in the ISM, but it seems that when the conditions are met, PNe can be important sources of fullerenes.

J.B.-S. acknowledges the support from a Marie Curie Intra-European Fellowship within the 7th European Community Framework Program under project number 272820. J.C., E.P., and E.M. acknowledge support from the Natural Sciences and Engineering Research Council of Canada (NSERC)

APPENDIX

FLUX MEASUREMENTS

We characterized the dust continuum by fitting a cubic spline through anchor points free of emission features along the

spectrum of each source (see Figure 1). We have not attempted to define the continuum beyond ∼25 μm because this position marks approximately the onset of the 30 μm feature, which usually extends beyond 40 μm. We quantified the amount of dust emission in each source by integrating the dust continua from 5 to 25 μm (see Table 1). We then measured the fluxes in the fullerene bands and estimated the associated uncertainties in the following way.

In the high-resolution spectrum of Tc 1, the strong [S III] line at 18.7 μm is much narrower than the broad fullerene emission band, and it is thus straightforward to determine its contribution to the flux in the emission band. The fullerene flux can thus be measured by simply integrating over the entire band and subtracting this [S III] contribution. The nominal uncertainty on the flux value obtained in this way is of the order of a percent. However, we feel that there is a larger source of uncertainty that originates from the positioning of the underlying continuum. To estimate this uncertainty, we fitted the observed band profile with three components: a broad Gaussian profile for the fullerene band,[8] a narrow Gaussian profile for the [S III] line, and a linear baseline that extends well beyond the band on both sides. In our best fit model, the uncertainty in the flux contained in this linear baseline is about 15% of the flux contained in the broad Gaussian representing the fullerene band, and represents a much larger uncertainty on our flux measurements since it is not clear whether the flux in our baseline really belongs to the continuum, or to the fullerene band (which would imply the true fullerene band profile is not Gaussian). Our best estimate for the fullerene flux thus includes half of the flux in this baseline. We note that we also expect C_{70} fullerenes to contribute to this band, and thus we subtracted the estimated C_{70} contribution (see Paper I) to finally obtain the C_{60} flux (see Table 1).

In the low-resolution observations of SMP SMC 16 and SMP LMC 56, the [S III] line does contribute to the 18.9 μm band, but it is much harder to separate from the fullerene band. Once again, we fitted the entire band using two Gaussian profiles and a linear baseline. This time though, we fixed the central wavelength of one component to the position of the [S III] line and its width to the instrumental resolution. Again, we can reproduce the observations quite well, and we follow the same approach as for Tc 1 to determine the fullerene flux and to estimate the uncertainty (see Table 1).

In the spectrum of Tc 1, the observed 17.4 μm band is not as symmetric as the 18.9 μm band, and shows some clear structure in its profile. Furthermore, there is weak emission in the red wing of the band amongst others due to a [P III] line at 17.88 μm; these, however, represent less than 10% of the total flux in the band. We still used a Gaussian fit to the band to estimate the uncertainty introduced by mispositioning the continuum; but since the band profile is asymmetric, we used the total integrated flux over the band (minus the contaminants and minus half the baseline flux) rather than the flux in the Gaussian fit as the best estimate for the fullerene flux. As before, we used the flux in the baseline as our uncertainty estimate. For SMP SMC 16 and SMP LMC 56, we could not estimate the contribution of the contaminants; therefore, the actual fullerene flux values are probably slightly lower than what we listed in Table 1; however, the contribution of these weak lines is probably smaller than the uncertainty on the flux value.

The 8.5 μm band was only observed at low resolution in all three sources. There are no clear contaminants, and in all three sources, the band can be well reproduced by a Gaussian profile (with possibly a small red wing asymmetry in the spectra of SMP SMC 16 and SMP LMC 56). For Tc 1, even the error introduced by continuum effects is very small; for the other sources, a slight red wing asymmetry is the largest source of uncertainty (of the order of 15%).

As was noted in Paper I, the observed 7.0 μm band in Tc 1 is a blend of C_{60} emission and an unresolved [Ar II] line that occurs at nearly the same wavelength. Thus, it was not clear what fraction of the emission band was due to C_{60}. Here, we tried the same approach as for the 18.9 μm band in the low-resolution spectra of SMP SMC 16 and SMP LMC 56: We carried out a two-component Gauss fit, where the central wavelength of one component is fixed to the position of the [Ar II] line and its width to the spectral resolution. In this way, we find that for Tc 1, most of the 7.0 μm emission band is in fact due to fullerenes; only about 15% of the flux is due to the [Ar II] line. This agrees well with an estimate for the [Ar II] flux obtained from the following abundance argument. Pottasch et al. (2011) compare Tc 1 to IC 418, and find that these two PNe are very similar in terms of excitation properties and physical conditions. However, while the ionic abundance of Ar^{++} is the same for both objects, that of Ar^{+} is 5.8 times higher in Tc 1 than in IC 418. Clearly, the discrepancy arises from the fact that the 7.0 μm flux was interpreted as pure [Ar II] emission and no contribution of C_{60} was taken into account. This then implies that the flux measured in the 7.0 μm band mostly originates from the fullerene band, and only about 1/6 of the emission is originating from the [Ar II] line, consistent with our measurements above. For SMP SMC 16, we similarly find that the [Ar II] flux is about 15% of the total emission in the band; for SMP LMC 56, however, the best fit solution has no contribution of [Ar II] (see Table 1). For this band, the uncertainty on the baseline is small, and the uncertainty on the flux values is dominated by the noise on the observations.

[8] As was noted already in Paper I, the 18.9 μm fullerene band is fairly symmetric, and can be well reproduced by a Gaussian profile.

REFERENCES

Allamandola, L. J., Tielens, G. G. M., & Barker, J. R. 1989, ApJS, 71, 733
Bakes, E. L. O., Tielens, A. G. G. M., & Bauschlicher, C. W., Jr. 2001, ApJ, 556, 501
Bauschlicher, C. W., Boersma, C., Ricca, A., et al. 2010, ApJS, 189, 341
Bernard-Salas, J., Peeters, E., Sloan, G. C., et al. 2009, ApJ, 699, 1541
Bernard-Salas, J., Pottasch, S. R., Wesselius, P. R., & Feibelman, W. A. 2003, A&A, 406, 165
Bernard-Salas, J., & Tielens, A. G. G. M. 2005, A&A, 431, 523
Berné, O., & Tielens, A. G. G. M. 2012, Proc. Natl. Acad. Sci., 109, 401
Buss, R. H., Jr., Cohen, M., Tielens, A. G. G. M., et al. 1990, ApJ, 365, L23
Cami, J., Bernard-Salas, J., Peeters, E., & Malek, S. E. 2010, Science, 329, 1180
Cami, J., Bernard-Salas, J., Peeters, E., & Malek, S. E. 2011, in IAU Symp. 280, The Molecular Universe, ed. J. Cernicharo & R. Bachiller (Cambridge: Cambridge Univ. Press), 216
Chase, B., Herron, N., & Holler, E. 1992, J. Phys. Chem., 96, 4262
Choi, C. H., Kertesz, M., & Mihaly, L. 2000, J. Phys. Chem. A, 104, 102
Clayton, G. C., De Marco, O., Whitney, B. A., et al. 2011, AJ, 142, 54
d'Hendecourt, L., Léger, A., Boissel, P., & Désert, F. 1989, in IAU Symp. 135, Interstellar Dust, ed. L. J. Allamandola & A. G. G. M. Tielens (Dordrecht: Kluwer), 207
Dopita, M. A., & Meatheringham, S. J. 1991, ApJ, 367, 115
Duley, W. W., & Williams, D. A. 2011, ApJ, 737, L44
Evans, A., van Loon, J. T., Woodward, C. E., et al. 2012, MNRAS, 421, L92
Fabian, J. 1996, Phys. Rev. B, 53, 13864
Foing, B. H., & Ehrenfreund, P. 1994, Nature, 369, 296
Fulara, J., Jakobi, M., & Maier, J. 1993, Chem. Phys. Lett., 211, 227
García-Hernández, D. A., Iglesias-Groth, S., Acosta-Pulido, J. A., et al. 2011a, ApJ, 737, L30
García-Hernández, D. A., Kameswara Rao, N., & Lambert, D. L. 2011b, ApJ, 729, 126

García-Hernández, D. A., Manchado, A., García-Lario, P., et al. 2010, ApJ, 724, L39
Gielen, C., Cami, J., Bouwman, J., Peeters, E., & Min, M. 2011, A&A, 536, A54
Higdon, S. J. U., Devost, D., Higdon, J. L., et al. 2004, PASP, 116, 975
Hony, S., Waters, L. B. F. M., & Tielens, A. G. G. M. 2002, A&A, 390, 533
Houck, J. R., Roellig, T. L., van Cleve, J., et al. 2004, ApJS, 154, 18
Iglesias-Groth, S. 2004, ApJ, 608, L37
Iglesias-Groth, S. 2006, MNRAS, 368, 1925
Iglesias-Groth, S., Cataldo, F., & Manchado, A. 2011, MNRAS, 413, 213
Jäger, C., Huisken, F., Mutschke, H., Jansa, I. L., & Henning, T. 2009, ApJ, 696, 706
Joblin, C., Toublanc, D., Boissel, P., & Tielens, A. G. G. M. 2002, Mol. Phy., 100, 3595
Jones, A. P. 2012a, A&A, 540, A1
Jones, A. P. 2012b, A&A, 540, A2
Jones, A. P. 2012c, A&A, 542, A98
Krätschmer, W., Fostiropoulos, K., & Huffman, D. R. 1990a, Chem. Phys. Lett., 170, 167
Krätschmer, W., Lamb, L. D., Fostiropoulos, K., & Huffman, D. R. 1990b, Nature, 347, 354
Kroto, H. W., Heath, J. R., Obrien, S. C., Curl, R. F., & Smalley, R. E. 1985, Nature, 318, 162
Kroto, H. W., & Jura, M. 1992, A&A, 263, 275
Kwok, S., Volk, K., & Bernath, P. 2001, ApJ, 554, L87
Lebouteiller, V., Bernard-Salas, J., Sloan, G. C., & Barry, D. J. 2010, PASP, 122, 231
Leisy, P., & Dennefeld, M. 2006, A&A, 456, 451
Micelotta, E., Jones, A., Cami, J., et al. 2012, ApJ, submitted
Peeters, E., Tielens, A. G. G. M., Allamandola, L. J., & Wolfire, M. G. 2012, ApJ, 747, 44
Perea-Calderón, J. V., García-Hernández, D. A., García-Lario, P., Szczerba, R., & Bobrowsky, M. 2009, A&A, 495, L5
Pottasch, S. R., Surendiranath, R., & Bernard-Salas, J. 2011, A&A, 531, A23
Roberts, K. R. G., Smith, K. T., & Sarre, P. J. 2012, MNRAS, 421, 3277
Rubin, R. H., Simpson, J. P., O'Dell, C. R., et al. 2011, MNRAS, 410, 1320
Scott, A., Duley, W. W., & Pinho, G. P. 1997, ApJ, 489, L193
Sellgren, K., Uchida, K. I., & Werner, M. W. 2007, ApJ, 659, 1338
Sellgren, K., Werner, M. W., Ingalls, J. G., et al. 2010, ApJ, 722, L54
Speck, A. K., Corman, A. B., Wakeman, K., Wheeler, C. H., & Thompson, G. 2009, ApJ, 691, 1202
Speck, A. K., Thompson, G. D., & Hofmeister, A. M. 2005, ApJ, 634, 426
Stanghellini, L., García-Lario, P., García-Hernández, D. A., et al. 2007, ApJ, 671, 1669
Stanghellini, L., Lee, T. H., Shaw, R. A., Balick, B., & Villaver, E. 2009, ApJ, 702, 733
Vassiliadis, E., & Wood, P. R. 1994, ApJS, 92, 125
Villaver, E., Stanghellini, L., & Shaw, R. A. 2003, ApJ, 597, 298
Volk, K., Hrivnak, B. J., Matsuura, M., et al. 2011, ApJ, 735, 127
Watson, R. A., Rebolo, R., Rubiño-Martín, J. A., et al. 2005, ApJ, 624, L89
Werner, M. W., Roellig, T. L., Low, F. J., et al. 2004, ApJS, 154, 1
Zhang, Y., & Kwok, S. 2011, ApJ, 730, 126